Acta Polytechnica **58**(1):69–76, 2018
doi:10.14311/AP.2018.58.0069

available online at http://ojs.cvut.cz/ojs/index.php/ap

H_2 PERMEATION BEHAVIOR OF Cr_2AlC AND Ti_2AlC MAX PHASE COATED ZIRCALOY-4 BY NEUTRON RADIOGRAPHY

Chongchong Tang[a], Mirco Grosse[a,*], Pavel Trtik[b], Martin Steinbrueck[a], Michael Stueber[a], Hans Jürgen Seifert[a]

[a] *Karlsruhe Institute of Technology, Germany / Institute for Applied Materials*

[b] *Laboratory for Neutron Scattering and Imaging, Paul Scherrer Institut, CH-5232 Villigen, Switzerland*

[*] corresponding author: Mirco.Grosse@kit.edu

Abstract. Hydrogen uptake by nuclear fuel claddings during normal operation as well as loss of coolant during design basis and severe accidents beyond design basis has a high safety relevance because hydrogen degrade the mechanical properties of the zirconium alloys applied as cladding material. Currently, claddings with enhanced accident tolerance are under development. One group of such accident tolerant fuel (ATF) claddings are zirconium alloys with surface coatings reducing corrosion and high-temperature oxidation rate, as well as the chemical heat and hydrogen release during hypothetical accidents. The hydrogen permeation through the coating is an important parameter ensuring material safety. In this work, the hydrogen permeation of Ti_2AlC and Cr_2AlC MAX phase coatings on Zircaloy-4 is investigated by means of neutron radiography. Both coatings are robust hydrogen diffusion barriers that effectively suppress hydrogen permeation into the matrix.

Keywords: MAX phase coating; Zircaloy; ATF; hydrogen permeation; neutron radiography.

1. Introduction

Worldwide many efforts are made after the Fukushima accident in 2011 to develop nuclear fuel components with enhanced accident tolerance. Aim of this research is the identification and qualification of fuel – cladding systems with increased time to failure during severe accident scenarios in nuclear reactors compared to the currently used system UO_2 fuel with claddings made of Zr-Sn like Zircaloy-2 and Zircaloy-4 (Zry-4), Zr-Nb like M5^{TM} and E110 or Zr-Sn-Nb alloys like ZIRLO® [1]. Besides the improvement of fuel properties like thermal conductivity, claddings with improved oxidation performance at temperatures of 1200 °C and above are under development. Such materials should enlarge the time until failure significantly by decreasing the release of hydrogen and chemical heat from the reaction with hot steam and/or by increasing the failure temperature, for instance the melting point [2]. Generally, three classes of materials are discussed [1, 3]:

- metallic claddings made for instance of FeCrAl alloys, showing significant lower oxidation rate with high-temperature steam along with a much lower chemical heat and hydrogen release;
- ceramic claddings made for instance of SiC with lower reaction rate and higher melting point; or
- zirconium alloys coated with materials owning lower reaction rate like chromium or MAX phases.

At KIT a PVD process was developed to produce Ti_2AlC and Cr_2AlC MAX phase coatings on Zircaloy-4 [4]. In the framework of characterization of the material compounds, various methods were applied including for instance X-ray diffraction (XRD), scanning electron microscopy (SEM), transmission electron microscopy (TEM) and oxidation experiments in steam at temperatures up to 1500 °C. An important property of the coatings is the permeability for hydrogen at operation temperature (∼350 °C) and during accident scenarios because hydrogen dramatically degrades the mechanical properties of zirconium alloys.

Hydrogen uptake in zirconium alloy can be studied quantitatively by means of neutron imaging as shown by various groups [5–8]. First neutron radiography investigations of the hydrogen permeability through Ti_2AlC and Cr_2AlC MAX phase coatings on Zry-4 are described in this paper.

2. Experimental

2.1. Preparation of MAX phase coated samples

Solid cylinder Zry-4 alloy specimens (1.5 wt% Sn, 0.2 wt% Fe, 0.1 wt% Cr, balance: Zr) with diameter of 12 mm and 14 mm height were used as substrates. In order to suppress hydrogen uptake of the Zry-4, the substrate specimens were pre-oxidized at 1173 K and normal pressure for 30 min in Ar/O_2 atmosphere to produce a dense ZrO_2 oxide layer of around 30 µm thickness [9]. The pre-oxidized layer can effectively suppress the hydrogen uptake besides the uncoated area during hydrogen permeation experiments [9]. The oxide layer was removed at one base plane of the cylinders by mechanical grinding and polishing allowing hydrogen uptake through this plane. Then the Ti_2AlC and Cr_2AlC MAX phase coatings, respectively, were

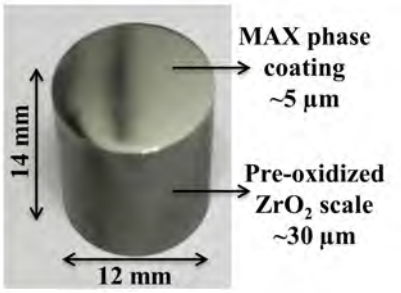

Figure 1. Ti_2AlC MAX phase coated Zircaloy-4 specimen for H_2 permeation experiments.

deposited on this polished base plane by non-reactive magnetron sputtering using three cylindrical elemental targets of titanium or chromium, respectively, graphite and aluminum with a Leybold Z 550 PVD equipment. An elemental nanoscale multilayer design, followed by thermal annealing at normal pressure in pure argon atmosphere was adopted to prepare the MAX phase coatings. The base pressure of the PVD chamber was around $1 \cdot 10^{-4}$ Pa and the Ar gas working pressure during deposition was maintained at 0.5 Pa, respectively. The substrates were plasma-etched with R.F. power of 500 W for 15 min prior to deposition. All three sputtering targets were operated at a target power of 200 W. During deposition, the substrate samples were grounded (i.e., no substrate bias voltage was applied). The nanoscale multilayer coatings were prepared by a well-defined process of substrate sample and shutter rotation. The annealing temperatures were 800 °C and 550 °C for Ti_2AlC and Cr_2AlC coatings, respectively. These temperatures have been identified to be appropriate for the formation of single-phase crystalline MAX phase structures. The dwell time was 10 min. The detailed process description on the synthesis of the Ti_2AlC MAX phase coatings can be found elsewhere [10]. The process parameters applied for the Cr_2AlC MAX phase coating are similar. Figure 1 depicts exemplarily the size and topography of one Ti_2AlC coated cylinder Zircaloy-4 alloy specimen. The phase composition and microstructure of the coatings were investigated and verified by X-ray diffraction (XRD, Seifert PAD II) and scanning electron microscopy (SEM, Philips XL30S), respectively.

2.2. H_2 permeation experiments

The H_2 permeation experiments were conducted using the so-called BOX furnace at KIT [11] with a horizontal corundum tube (inner diameter 40 mm). The cylinder specimen stood on an alumina boat that was placed at the center of the furnace. The specimen was first heated in pure argon atmosphere with Ar flow rate of 20 l/h and 10 K/min heating rate to the desired temperatures, then the atmosphere was changed to Ar with 5 vol% H_2 with the same flow rate for H_2 permeation. Following the isothermal annealing in Ar/H_2, the atmosphere was switched back to pure argon and the specimen was cooled down to room temperature in the furnace. The H_2 permeation experiments were run at several temperatures, including 800 °C, 700 °C, 500 °C and 350 °C. In principal, the coatings will undergo corrosion or oxidation during practical application. In order to determine the H_2 permeation behavior through oxidized coatings, some of the coated samples were pre-oxidized at 800 °C under normal pressure for 1 hour in Ar/O_2 atmosphere before H_2 permeation experiments. Uncoated Zircaloy-4 specimen was treated on the same way as reference.

2.3. Neutron radiography

Neutron radiography experiments were performed at the ICON neutron imaging facility at the Swiss spallation neutron source SINQ at PSI Villigen, Switzerland [12] using a cold neutron spectrum. The micro-tomography setup consists of an ANDOR detector with 13.5 µm pixel distance. A field of view of 28×28 mm and a beam collimation of $L/D \approx 340$ were applied. The distance between the 20 µm thick Gadox scintillator screen and the sample was about 5 mm. In order to detect small hydrogen concentrations, the median of 11 to 166 images of 60 s individual acquisition times were determined using the ImageJ software. This procedure suppresses white spots in the image caused by high energetic γ quants.

The quantitative correlation between hydrogen concentration in terms of N_H/N_{Zr} atomic number ratio and total macroscopic neutron cross section Σ_{total} were determined by measuring of cladding tub segments with known hydrogen concentration as described in [5]:

$$\Sigma_{total} = \frac{-\ln \frac{I-I_B}{I_0-I_B}}{s} \sum_i N_i \sigma_i = \Sigma_{total,\ sample\ as\ received} + N_H \sigma_H, \quad (1)$$

where I, I_0 and I_B are the intensity with sample, without sample and the background intensity, respectively; N_i is the number density and σ_i is the total microscopic neutron cross section of the isotope i. Because $N_H\sigma_H = \frac{N_H}{N_{Zr}} N_{Zr}\sigma_H$, the dependence of Σ_{total} on N_H/N_{Zr} is linear and can be written as

$$\Sigma_{total} = A + B\frac{N_H}{N_{Zr}} \quad (2)$$

with $A = \Sigma_{total,\ sample\ as\ received}$ and $B = N_{Zr}\sigma_H$ Figure 2 plots the calibration curve measured in this beam time. The following correlation was determined:

$$\Sigma_{total} = 0.222 + 2.153\frac{N_H}{N_{Zr}}. \quad (3)$$

3. Results and discussion

3.1. Microstructure of MAX phase coatings

Single-phase and dense Ti_2AlC and Cr_2AlC MAX phase coatings can be synthesized following the two-

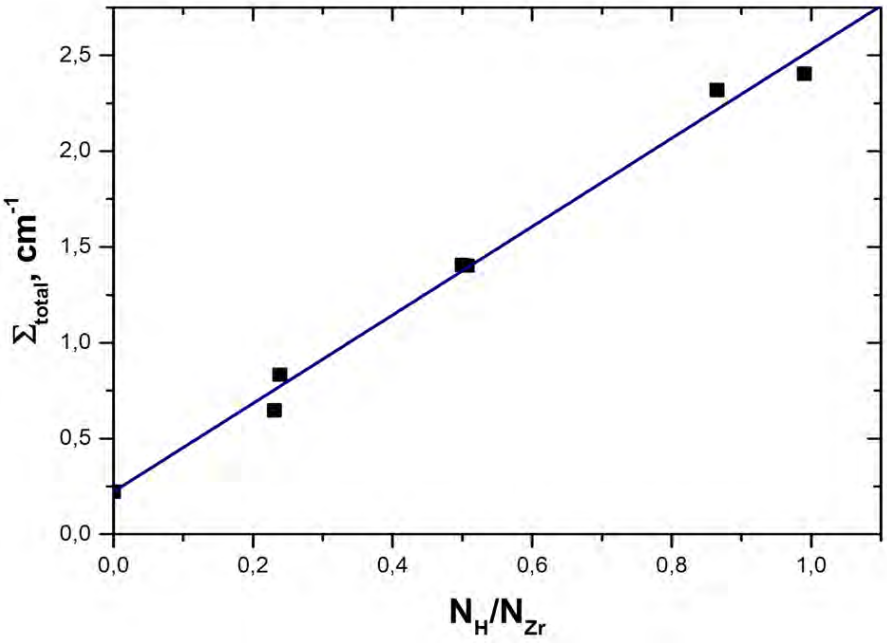

FIGURE 2. Calibration curve of the dependence of the total macroscopic neutron cross section Σ_{total} on the atomic number density ratio between hydrogen and zirconium $N_{\text{H}}/N_{\text{Zr}}$.

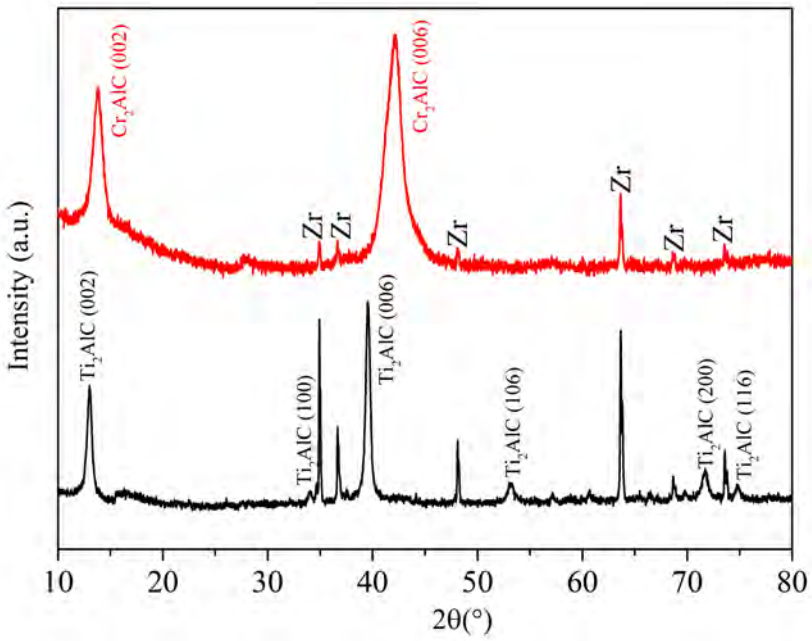

FIGURE 3. XRD patterns of Ti_2AlC (bottom) and Cr_2AlC (top) MAX phase coatings on Zry-4 substrates by annealing of as-deposited elemental nanoscale multilayers.

step processes described above in this study. Figure 3 shows the XRD patterns of Ti_2AlC and Cr_2AlC MAX phase coatings on Zry-4 substrates after annealing of the as-deposited elemental nanoscale multilayers at 800 °C and 550 °C, respectively, for 10 min in argon. Both type of samples show only XRD signals attributable to either the Ti_2AlC or Cr_2AlC MAX phases and the Zircaloy-4 substrate. All diffraction signals that can be indexed to Ti_2AlC (JCPDS card No. 29-95) and Cr_2AlC (JCPDS card No. 29-17) MAX phases are shown in Fig.3. However, the crystallinity of both MAX phase materials is slightly different. While both coatings show significant differences in crystallite size probably stemming from their different annealing temperatures, the Ti_2AlC coatings show XRD signals of various lattice planes (polycrystalline growth with basal-plane preferred orientation) and the Cr_2AlC coatings show mainly signals of basal-plane (tendency to textured growth). All other diffraction signals are related with the Zircaloy-4 substrate (their position is indicated only for the XRD pattern of the Cr_2AlC coated sample). Common competing phases,

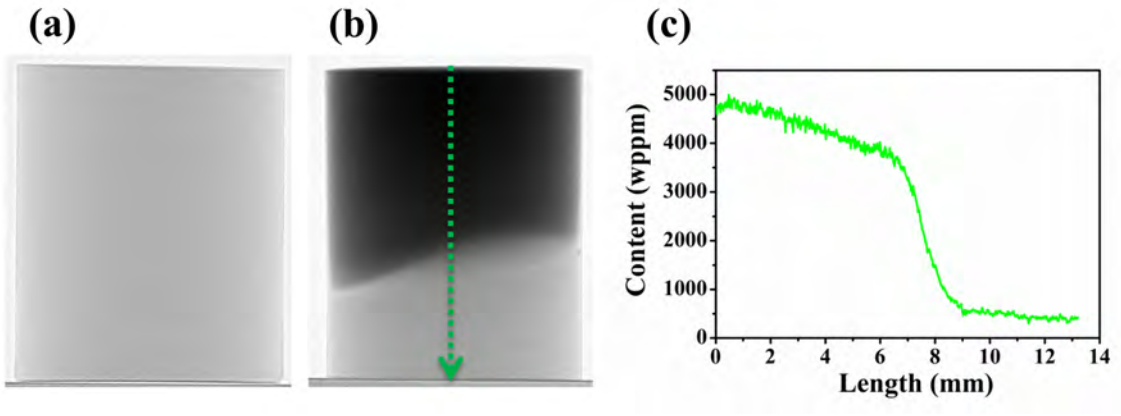

Figure 5. Neutron radiography images of the reference uncoated Zircaloy-4 specimens (a) before hydrogen loading and (b) after hydrogen permeation at 700 °C for 1 h (hydrogen dark). (c) Hydrogen distribution profile along cylinder axis from top to bottom in (b).

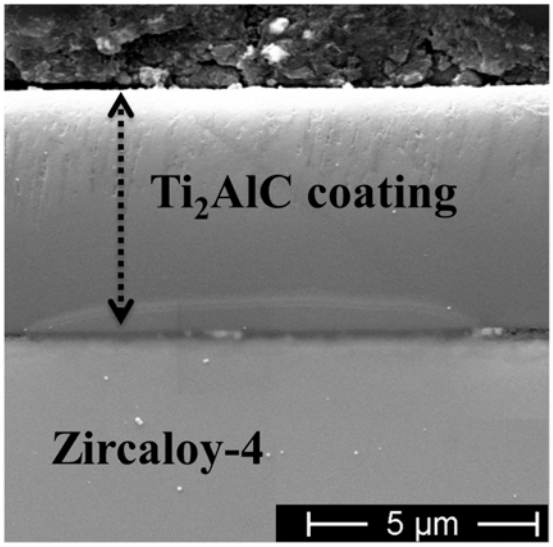

Figure 4. SEM images of cross-section view of Ti_2AlC coating on Zry-4.

like binary carbides and intermetallics [13], that could occur during preparation of the MAX phase coatings by magnetron sputtering and post-annealing were not detected by XRD. The cross-sectional SEM image of the Ti_2AlC MAX phase coating is shown in Figure 4 as an example. It can be seen that the coating is dense and uniform, as well as free of large growth defects. The thickness of the coating is around 5.1 µm. Few tiny cracks were observed on the surface of the Cr_2AlC coatings (not shown here) after annealing probably due to the different thermal expansion coefficients between coating and substrate. However, the cracks do not penetrate into the substrate.

3.2. H_2 permeation of unoxidized coatings

Uncoated Zircaloy-4 specimens before and after hydrogenation were examined as reference and the results are displayed in Figure 5. Figure 5ab shows the neutron radiography images of the uncoated Zircaloy-4 specimens before hydrogen loading and after hydrogenation at 700 °C for 1 h, respectively. The same brightness and contrast settings were applied for all radiography images in order to give a straightforward visual inspection for comparing the hydrogen content. The pristine Zry-4 specimen appears homogeneously bright due to the high neutron transmission. In contrast, after thermal annealing in hydrogen atmosphere significant amount of hydrogen penetrated into the cylinder through the polished plane and the hydrogen containing regions became much darker (Figure 5b). The diffusion front is clearly visible. Figure 5c illustrates the hydrogen distribution profile along the cylinder axis. The hydrogen concentration reached 5000 wppm at the gas/alloy interface. The lower regions of the cylinder loaded with hydrogen showed similar brightness compared to the pristine specimen. Thus, no obvious hydrogen penetration through the pre-oxidized ZrO_2 scale was detected.

Figure 6 presents neutron radiography images of Cr_2AlC and Ti_2AlC coated Zircaloy-4 specimens after annealing in Ar/H_2 at 800 °C for 1 h. Figure 6c plots the hydrogen distribution profiles along the cylinder axis. The images apparently reveal that both coatings are robust barriers against hydrogen permeation. The brightness of Figure 6ab is on the same level compared to the pristine specimens (Figure 5a). The quantitative analysis given in Figure 6c shows a homogeneous hydrogen distribution profile along the cylinder axis without any gradients. The determined averaged hydrogen concentrations are very low, about 50 wppm for the Ti_2AlC coating and only about 10 wppm for Cr_2AlC coated Zircaloy-4. It has to be taken into account that the values are determined by Eq. (1c) based on the model that only the hydrogen concentration is changed. Processes slightly increasing the total macroscopic neutron cross section too like the diffusion of oxygen from the oxide layer or atoms from the coating into the metal are not considered. Therefore,

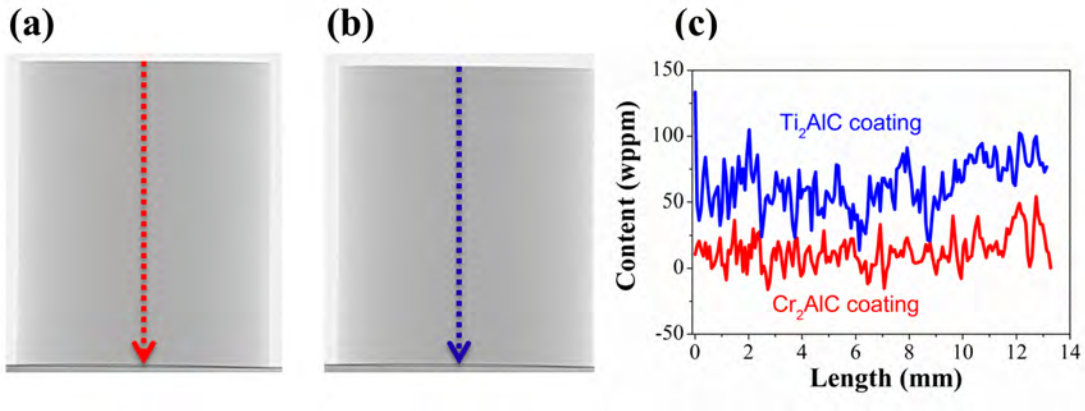

FIGURE 6. Neutron radiography images of (a) Cr_2AlC and (b) Ti_2AlC coated Zircaloy-4 specimens after hydrogen permeation at 800 °C for 1 h. (c) Hydrogen distribution profiles along cylinder axis from top to bottom in (a) and (b).

the absence of a gradient in the hydrogen distribution proves that no hydrogen uptake through the coating occurred even the averaged value is not exactly zero. It has to be mentioned that the scattering of the values are not caused by the counting statistics in the neutron radiography experiment. The scattering cannot be reduced by re-binning of the detector pixels. It shows that the fluctuations in the hydrogen concentrations determined are caused by local material fluctuations. It can be concluded that the ∼5 µm MAX phase coatings are just as effective as the pre-oxidized 30 µm ZrO_2 layer suppressing hydrogen uptake into the matrix.

The hydrogen diffusion rate through the MAX phase coatings cannot be calculated based on Fick's diffusion law since no hydrogen concentration gradient was observed. The hydrogen permeation rate can be estimated by the following definition

$$\text{Ø} = \frac{\Delta M}{St}, \tag{4}$$

where Ø is the hydrogen permeation rate at a certain temperature, ΔM is the mass gain due to hydrogen absorption, S is the exposure area and t is the permeation time. Assuming that the hydrogen concentration is at the magnitude of 10^1 ppm for the MAX phase coated Zircaloy-4 specimens after hydrogen permeation at 800 °C for 1 h, the hydrogen permeation rate through the uncoated and coated surfaces can be compared. The estimated rate is around $6.6 \cdot 10^{-2}\,\mathrm{g\,m^{-2}\,s^{-1}}$ for uncoated Zircaloy-4 at 700 °C; in contrast, it descends to around $10^{-4}\,\mathrm{g\,m^{-2}\,s^{-1}}$ for MAX phase coated specimens even at higher temperature 800 °C. It is necessary to mention that the maximal permeation rate estimated here is based on very low average values of the hydrogen concentrations being below their point-to-point scattering as shown in Figure 6c. Hence, the ∼5 µm MAX phase layer reduced the hydrogen permeation rate at least by about two orders of magnitudes or more.

It is well known that various coatings, mainly oxide, nitride, and carbide ceramics, on structural components have been examined extensively as hydrogen permeation barriers [14]. These ceramics usually have very low permeability for hydrogen isotopes caused by their low hydrogen solubility and diffusivity. Previous studies also confirmed that finely dispersed carbides in a steel matrix act as deep trapping sites to retain hydrogen that might otherwise diffuse through [15, 16]. Trapping of hydrogen fairly reduces the apparent hydrogen diffusion rates in the matrix; meanwhile, the hydrogen isotopes are restricted to the interior lattice structure of the carbides. Recent first-principle theoretical calculations demonstrated that hydrogen interstitial atoms are preferably and as readily to be incorporated into the interstitial sites of Ti-Al layers in stoichiometric Ti_3AlC_2 or C vacancies in C-deficient Ti_3AlC_2 MAX phase [17, 18]. Due to MAX phases share similar lattice structure, above calculated configurations of hydrogen trapping sites are suggested also applying for the two 211-MAX phases, Ti_2AlC and Cr_2AlC. The trap of hydrogen atoms in interstitial or vacancy sites probably can drastically impede the permeation of hydrogen and reduce the hydrogen partial pressure at the MAX phase coating/substrate interface.

Another important factor determining the barrier efficiency is the microstructural integrity [14, 19]. Thus, barriers that can provide a sufficient permeation reduction should be essentially free of various defects. In general, grain boundaries featured by the typical columnar structure of coatings deposited by PVD or other macroscale defects including cracks and voids that act as short-circuit diffusion path can significantly reduce the barrier efficiency. However, by adopting a two-step synthesis process, the MAX phase coatings in this study are dense, consisting of nano-crystalline grains without columnar growth [10]. The unique microstructural features of the coatings can improve the efficiency in limiting hydrogen permeation as a barrier.

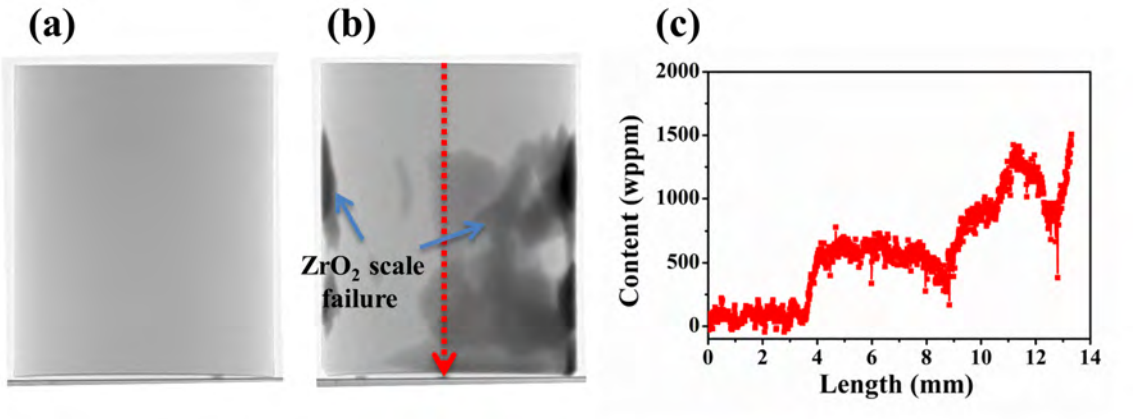

Figure 7. Neutron radiography images of pre-oxidized Cr_2AlC coated Zircaloy-4 specimens after hydrogen permeation at (a) 700 °C and (b) 500 °C for 1 h (hydrogen dark). (c) Hydrogen distribution profile along cylinder axis from top to bottom in (b).

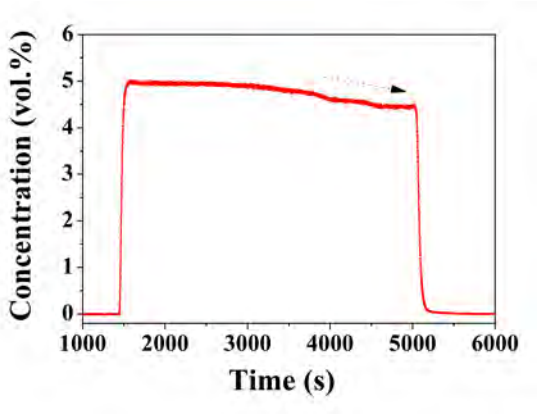

Figure 8. Hydrogen concentration in the off-gas during hydrogen permeation of pre-oxidized Cr_2AlC coated Zircaloy-4 specimens at 500 °C for 1 h. A decrease of the hydrogen concentration was shown due to fast permeation through locally failed ZrO_2 scale.

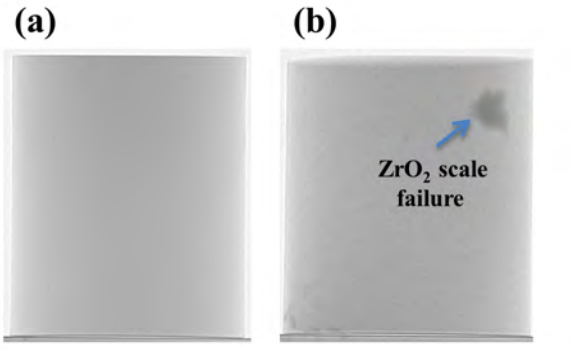

Figure 9. Neutron radiography images of pre-oxidized Ti_2AlC coated Zircaloy-4 specimens after hydrogen permeation at (a) 700 °C and (b) 500 °C for 1 h (hydrogen dark).

3.3. H_2 permeation of oxidized coatings

Figure 7 displays the results of pre-oxidized Cr_2AlC coated Zircaloy-4 specimens after hydrogen permeation at two different temperatures (700 and 500 °C). The neutron radiography images after annealing in hydrogen atmosphere at 700 °C for 1 hour (Figure 7a) shows similar brightness levels compared to the as-received specimen (Figure 5a) and the coated, unoxidized ones (Figure 6a). No obvious dark regions can be observed. For the specimen after annealing at 500 °C for 1 hour, localized failure of the ZrO_2 layer through crack and spallation is found (Figure 6b). Hydrogen penetrated aggressively through the failure areas and the hydrogen containing area appeared darker. The hydrogen distribution profile (Figure 7c) proves that in the upper part of the specimens where the coating is located and less oxide layer failures exist, the hydrogen concentration is close to zero, just around dozens of wppm. Figure 8 shows the evolution of the hydrogen concentration in the off-gas during hydrogen permeation at 500 °C. The hydrogen concentration remained constant, then decreased gradually after certain exposure time associated with the localized failure of the ZrO_2 layer. The reason leading to the failure of the ZrO_2 layer is the diffusion of oxygen from the oxide into the metal. It seems to be enhanced by treatment during grinding and polishing and is accelerated by the local material swelling after first local hydrogen uptakes. In all permeation tests, during which the ZrO_2 layer survived, the hydrogen concentration in the off-gas flow always remained constant.

The pre-oxidized Ti_2AlC coatings were proved as effective as the pre-oxidized Cr_2AlC coatings in limiting the hydrogen permeation as shown in Figure 9. No dark areas enriched in hydrogen were observed except for one small region after 500 °C exposure where the ZrO_2 layer failed. It is hard to determine which coating suppresses the hydrogen uptake more efficiently. No hydrogen absorption of the substrate above the detection limits was observed for both coatings. Annealing of both pre-oxidized coatings in hydrogen atmosphere at 350 °C for 4 h (not shown here) revealed no indication of mass change, and the hydrogen concentration determined by quantitative analysis appeared below 1 wppm.

Oxidation of Ti_2AlC and Cr_2AlC coatings lead to the growth of oxide scale on the surface. Ti_2AlC coated Zircaloy-4 fabricated by same process during oxidation at 800 °C grew a scale consisting of two sublayers: an outer dense alumina-rich layer and an inner porous titania layer as former own investigations have demonstrated [4]. In general, the oxidation of Cr_2AlC coatings result in the formation of an alumina-rich scale at relatively low temperature or a dense continuous oxide scale consisting of alumina on Cr carbides at high temperature [20, 21]. Alumina, particularly the α-phase of aluminium oxide (corundum) and chromia are robust hydrogen permeation barriers that can reduce the permeation rate by three orders of magnitude in laboratory experiments [22, 23]. Thus, it can be expected that both pre-oxidized MAX phase coatings can serve as satisfactory barriers for limiting hydrogen isotope permeation.

4. Conclusions

Neutron radiography investigations have demonstrated that this method is appropriate to measure the hydrogen permeability of coatings on zirconium alloys. The uncertainty of the hydrogen permeation rate through the coatings is given by the detection limit of hydrogen concentration in zirconium alloys using neutron radiography. In case of the experiments of this study it is in the order of magnitude of $10^{-4}\,\mathrm{g\,m^{-2}\,s^{-1}}$.

Both, the Ti_2AlC and Cr_2AlC MAX phase coatings suppress hydrogen uptake effectively. Their permeation rate is below the detection limit given before. The ∼5 µm MAX phase coatings are as effective as the pre-oxidized 30 µm ZrO_2 layer suppressing hydrogen permeation into the matrix.

Problems in the determination of the hydrogen uptake through the coatings were caused by failures in the oxide layer produced by pre-oxidation. To overcome this problem the authors recommend oxidizing the samples after deposition and final heat treatment of the coatings. New methodical developments, such as high-resolution neutron imaging [24] may improve the power of neutron radiography for measuring hydrogen permeation rates through coatings at zirconium alloys.

Acknowledgements

The Helmholtz (HGF) programs NUSAFE and STN at the Karlsruhe Institute of Technology supported this work. C. Tang thanks the PhD fellowship funded by the China Scholarship Council (CSC). The authors also thank Mr. S. Zils for technical support during coating deposition. The work on MAX phase coatings was carried out with the support of the Karlsruhe Nano Micro Facility (KNMF, `www.knmf.kit.edu`), a Helmholtz research infra- structure at Karlsruhe Institute of Technology (KIT, `www.kit.edu`). The neutron radiography investigations were performed at the ICON facility at PSI Villigen, Switzerland. The authors thank PSI for providing 24 h beam time for these investigations.

References

[1] Duan, Z., Yang, H., Satoh, Y., Murakami, K., Kano, S., Zhao, Z., Shen, J., Abe, H.: Current status of materials development of nuclear fuel cladding tubes for light water reactors. *Nucl. Eng. Des.*, **316**, 2017, p. 131–150. DOI:10.1016/j.nucengdes.2017.02.031

[2] Zinkle, S.J., Terrani, K.A., Gehin, J.C., Ott, L.J., Snead, L.L.: Accident tolerant fuels for LWRs: A perspective. *J. Nucl. Mater.*, **448** (1–3), 2014, p. 374–379. DOI:10.1016/j.jnucmat.2013.12.005

[3] Tang, C., Stueber, M., Seifert, H.J., Steinbrueck, M.: Protective coatings on zirconium-based alloys as accident-tolerant fuel (ATF) claddings. *Corros. Rev.*, **35** (3), 2017, p. 141–166. DOI:10.1515/corrrev-2017-0010

[4] Tang, C., Stueber, M., Steinbrueck, M., Grosse, M., Ulrich, S., Seifert, H.J.: *Assessment of high-temperature steam oxidation behavior of Zircaloy-4 with Ti2AlC coating deposited by magnetron sputtering.* In: The Nuclear Materials Conference. 2016.

[5] Grosse, M., Lehmann, E., Vontobel, P., Steinbrueck, M.: Quantitative determination of absorbed hydrogen in oxidised zircaloy by means of neutron radiography. *Nucl. Instruments Methods Phys. Res. Sect. A Accel. Spectrometers, Detect. Assoc. Equip.*, **566** (2), 2006, p. 739–745. DOI:10.1016/j.nima.2006.06.038

[6] Wang, Z., Garbe, U., Li, H., Harrison, R.P., Kaestner, A., Lehmann, E.: Observations on the Zirconium Hydride Precipitation and Distribution in Zircaloy-4. *Metall. Mater. Trans. B*, **45** (2), 2014, p. 532–539.

[7] Brachet, J.C., Hamon, D., Le Saux, M., Vandenberghe, V., Toffolon-Masclet, C., Rouesne, E., Urvoy, S., Béchade, J.L., Raepsaet, C., Lacour, J.L., Bayon, G., Ott, F.: "Study of secondary hydriding at high temperature in zirconium based nuclear fuel cladding tubes by coupling information from neutron radiography/tomography, electron probe micro analysis, micro elastic recoil detection analysis and laser induced breakdow. *J. Nucl. Mater.*, **488**, 2017, p. 267–286.

[8] Smith, T., Bilheux, H., Ray, H., Bilheux, J.C., Yan, Y.: High Resolution Neutron Radiography and Tomography of Hydrided Zircaloy-4 Cladding Materials. *Phys. Procedia*, **69** (October 2014), 2015, p. 478–482.

[9] Grosse, M., Van Den Berg, M., Goulet, C., Kaestner, A.: In-situ investigation of hydrogen diffusion in Zircaloy-4 by means of neutron radiography. *J. Phys. Conf. Ser.*, **340**, 2012, p. 12106. DOI:10.1088/1742-6596/340/1/012106

[10] Tang, C., Klimenkov, M., Jaentsch, U., Leiste, H., Rinke, M., Ulrich, S., Steinbrück, M., Seifert, H.J., Stueber, M.: Synthesis and characterization of Ti_2AlC coatings by magnetron sputtering from three elemental targets and ex-situ annealing. *Surf. Coatings Technol.*, **309**, 2017, p. 445–455.

[11] M. Steinbrück, Stegmaier, U., Ziegler, T.: *Prototypical experiments relating to air oxidation of Zircalloy-4 at high temperatures.* Karlsruhe, 2007.

[12] Kaestner, A.P., Hartmann, S., Kühne, G., Frei, G., Grünzweig, C., Josic, L., Schmid, F., Lehmann, E.H.: The ICON beamline A facility for cold neutron imaging at SINQ. *Nucl. Instruments Methods Phys. Res. Sect. A Accel. Spectrometers, Detect. Assoc. Equip.*, **659** (1), 2011, p. 387–393.

[13] Eklund, P., Beckers, M., Jansson, U., Högberg, H., Hultman, L.: The Mn+1AXn phases: Materials science and thin-film processing. *Thin Solid Films*, **518** (8), 2010, p. 1851–1878. DOI:10.1016/j.tsf.2009.07.184

[14] Causey, R.A., Karnesky, R.A., San Marchi, C.: *Tritium Barriers and Tritium Diffusion in Fusion Reactors*. In: Comprehensive Nuclear Materials. 2012, p. 511–549.

[15] Takahashi, J., Kawakami, K., Tarui, T.: Direct observation of hydrogen-trapping sites in vanadium carbide precipitation steel by atom probe tomography. *Scr. Mater.*, **67** (2), 2012, p. 213–216.

[16] Chen, Y.-S., Haley, D., Gerstl, S.S.A., London, A.J., Sweeney, F., Wepf, R.A., Rainforth, W.M., Bagot, P.A.J., Moody, M.P.: Direct observation of individual hydrogen atoms at trapping sites in a ferritic steel. *Science (80-.).*, **355** (6330), 2017, p. 1196–1199.

[17] Ding, H., Glandut, N., Fan, X., Liu, Q., Shi, Y., Jie, J.: First-principles study of hydrogen incorporation into the MAX phase Ti_3AlC_2. *Int. J. Hydrogen Energy*, **41** (15), 2016, p. 6387–6393. DOI:10.1016/j.ijhydene.2016.03.015

[18] Xu, C., Zhang, H., Hu, S., Zhou, X., Peng, S., Xiao, H., Zhang, G.: First-principles calculations of Ti_3SiC_2 and Ti_3AlC_2 with hydrogen interstitial. *J. Nucl. Mater.*, **488**, 2016, p. 261–266.

[19] Li, Q., Wang, J., Xiang, Q.Y., Tang, T., Rao, Y.C., Cao, J.L.: Thickness impacts on permeation reduction factor of Er_2O_3 hydrogen isotopes permeation barriers prepared by magnetron sputtering. *Int. J. Hydrogen Energy*, **41** (4), 2016, p. 3299–3306. DOI:10.1016/j.ijhydene.2015.11.046

[20] Wang, Q.M., Flores Renteria, A., Schroeter, O., Mykhaylonka, R., Leyens, C., Garkas, W., to Baben, M.: Fabrication and oxidation behavior of Cr_2AlC coating on Ti_{6242} alloy. *Surf. Coatings Technol.*, **204** (15), 2010, p. 2343–2352.

[21] Hajas, D.E., to Baben, M., Hallstedt, B., Iskandar, R., Mayer, J., Schneider, J.M.: Oxidation of Cr_2AlC coatings in the temperature range of 1230 to 1410°C. *Surf. Coatings Technol.*, **206** (4), 2011, p. 591–598. DOI:10.1016/j.surfcoat.2011.03.086

[22] Hollenberg, G.W., Simonen, E.P., Kalinin, G., Terlain, A.: Tritium/hydrogen barrier development. *Fusion Eng. Des.*, **28** (C), 1995, p. 190–208. DOI:10.1016/0920-3796(95)90039-X

[23] Levchuk, D., Bolt, H., Döbeli, M., Eggenberger, S., Widrig, B., Ramm, J.: Al-Cr-O thin films as an efficient hydrogen barrier. *Surf. Coatings Technol.*, **202** (20), 2008, p. 5043–5047. DOI:10.1016/j.surfcoat.2008.05.012

[24] Trtik, P., Lehmann, E.H. Progress in high resolution neutron imaging at Paul Scherrer Institut – The Neutron Microscope Project, J. Phys. – Conf. Series., 746, 2016, 012004.